JOURNAL OF GUIDANCE, CONTROL, AND DYNAMICS
Vol. 34, No. 1, January–February 2011

Piloted Simulation Study Comparing Classical, H_∞, and Linear Parameter-Varying Control Methods

Daniel J. Alvarez*
Systems Technology, Inc., Hawthorne, California 90250
and
Bei Lu†
California State University, Long Beach, California 90840

DOI: 10.2514/1.50198

Piloted simulation is often regarded as an intermediate step between traditional desktop analysis and flight test. It is a valuable tool in the assessment of how changes in flight control system parameters affect closed-loop vehicle performance. This paper focuses on the piloted simulation evaluation of classical proportional-integral-derivative, robust H_∞, and linear parameter-varying control design methods. Three different controllers are designed for the longitudinal flight dynamics of the F-16 variable stability in-flight simulator test aircraft within a defined flight envelope. After assessing the performance of each controller using the desktop analysis and simulation, a piloted simulation study is provided to gather qualitative pilot ratings and comments to validate or refute the results and conclusions which were based on the preliminary desktop analysis. The pilot-in-the-loop flight simulator, simulation test plan, and controller evaluation procedure are described. The data obtained from a two-pilot simulation test are then used to conduct a full-handling-qualities study comparing the performance and robustness of each controller. The paper concludes with the selection of the controller that is best suited for application to a modern, fighter-type aircraft.

Nomenclature

k_q	=	proportional-integral compensator gain, dimensionless
q	=	pitch rate, deg/s
T_q	=	proportional-integral compensator zero, dimensionless
$T_{\theta 1}$, $T_{\theta 2}$	=	open-loop zeros of longitudinal mode, dimensionless
V	=	airspeed, kt
α	=	angle of attack, deg
γ	=	flight path angle, deg
δ_e	=	elevator deflection, deg
δ_{lon}	=	longitudinal stick input, dimensionless
δ_{th}	=	throttle input, dimensionless
θ	=	pitch attitude, deg
ζ_{P}, ζ_{SP}, ζ'_{SP}	=	damping ratio of open-loop phugoid, open-loop short period, or closed-loop short period modes, dimensionless
τ_e	=	effective time delay, s
τ_p	=	phase delay, s
ω_{BW}	=	bandwidth frequency, rad/s
$\omega_{n\text{P}}$, $\omega_{n\text{SP}}$, $\omega'_{n\text{SP}}$	=	natural frequency of open-loop phugoid, open-loop short period, or closed-loop short period modes, rad/s
ω_c	=	crossover frequency, rad/s

Presented as Papers 2010-7940 and 2010-7941 at the 2010 AIAA Atmospheric Flight Mechanics Conference, Toronto, ON, Canada, 2–5 August 2010; received 5 April 2010; revision received 10 August 2010; accepted for publication 24 August 2010.

*Staff Engineer, Research, 13766 South Hawthorne Boulevard; dalvarez@systemstech.com. Member AIAA.

†Assistant Professor, Department of Mechanical and Aerospace Engineering; blu3@csulb.edu. Member AIAA.

I. Introduction

FLIGHT control engineering can be broken into two distinct but inherently interrelated subdivisions: control design and analysis and the study of aircraft handling qualities. Control designers and analysts focus mostly on the vehicle itself; different control methods are developed and implemented to ensure a robust and well-performing system considering only the end-to-end vehicle response as the primary performance metric. Handling qualities engineers, however, are concerned with the pilot-vehicle system. It is the pilot who is the outermost feedback mechanism of a flight control system, and it is in this loop where aircraft stability and performance should be measured. The metrics used to gauge pilot-vehicle system performance are sometimes subjective; pilot ratings of handling qualities and tendency of the aircraft to enter a pilot-induced oscillation (PIO) when performing a task are two qualitative measurements of pilot opinion. These qualitative assessments are used in combination with the quantitative metrics derived from flight test data to assess the validity of the preliminary desktop analysis and ultimately determine the goodness of a design.

Though the theories used to design and analyze control systems have advanced in the past 50 years [1], the control methods and architectures employed on many modern aircraft have remained largely the same. Classical proportional-integral-derivative (PID) control systems are the standard for most aircraft due to their simple structure. Today, the existence of heavily instrumented test aircraft allows for complex control systems to be simulated in flight.

In recent years, robust design methods, such as H_∞ control, have been employed in an attempt to address the problem of aircraft instability in flight due to the lack of robustness offered by classical control. These techniques have proven to be particularly effective for systems whose dominant dynamics can be accurately captured by a single, linear time-invariant model [2,3]. For an aircraft maneuvering in a wide flight envelope, its dynamic behavior varies significantly during operation. Purely linear controllers are not able to effectively control highly maneuverable aircraft in a wide flight envelope. Traditionally, gain scheduling is incorporated into the controller implementation to ensure controller performance across the wide envelope. However, there are no stability and performance guarantees for interpolation between the point controllers [4]. Linear parameter-varying (LPV) control theory has been explored to

eliminate the problems with gain scheduling [5–7]. The LPV control method is an extension of H_∞ control theory for LPV systems which explicitly takes into account the relationship between real-time parameter variations and performance. This enables controllers to be designed for the entire range of operating conditions with theoretical guarantees of stability and performance throughout the region.

The research on robust flight control has offered valid control solutions which balance stability and performance for many platforms. However, most have typically addressed only one component of the flight control problem, focusing on the design of a controller and a subsequent desktop analysis. Of the few studies that have extended the analysis and controller assessment into the pilot-vehicle system through piloted simulation or flight test, almost all have been in an attempt to prove the viability of the robust controller. Even fewer have compared the performance of a flight controller designed with robust design methods against a classically-designed controller. The results of an extensive reference search found only one source which compared the stability and performance of classical and robust control using flight test results [8]. In [8], several controllers were developed using classical and H_2/H_∞ methods and a flight test using the Calspan VSS 2 Learjet was conducted. This research successfully brought three areas of interest in flight control engineering together: the use of robust control design techniques to design flight controllers for modern, high performance aircraft, the comparison of classical and robust control design methodologies, and the use of piloted simulation to append the quantitative analysis result with qualitative pilot opinion. However, it was lacking a formal handling qualities study in which pilots gave handling qualities and PIO tendency ratings in an assessment of each controller. The research presented in this paper hopes to expand and improve upon the comparisons made in [8] through the inclusion of pilot ratings and a thorough analysis of handling qualities data. In addition, it should be mentioned that the application of the LPV technique to flight control is still in the stage of desktop simulation and analysis. Another contribution of this paper is therefore to examine the applicability and effectiveness of the LPV control technique through piloted simulation.

The objectives of this paper are to provide a direct comparison of classical, H_∞, and LPV control design methods using both desktop analysis and a piloted simulation handling qualities study and to draw conclusions as to which design methodology offers superior closed-loop performance in a compensatory tracking task. The paper is organized as follows: Sec. II presents a survey of the F-16 VISTA model, which is used as the test vehicle for the study. The control design methods, including proportional-integral (PI) control, H_∞ control, and LPV control are described in Sec. III. Section IV offers a comparison of the closed-loop system performance for the three controller designs using desktop analysis. A piloted simulation study is given in Secs. V and VI to gather qualitative pilot ratings and comments to validate or refute the results and conclusions which were based on the preliminary desktop analysis. Section V presents a detailed description of the flight simulator, test plan and evaluation procedures. The results of the flight test and subsequent handling qualities analysis are presented in Sec. VI. Section VII offers a summary and draws final conclusions.

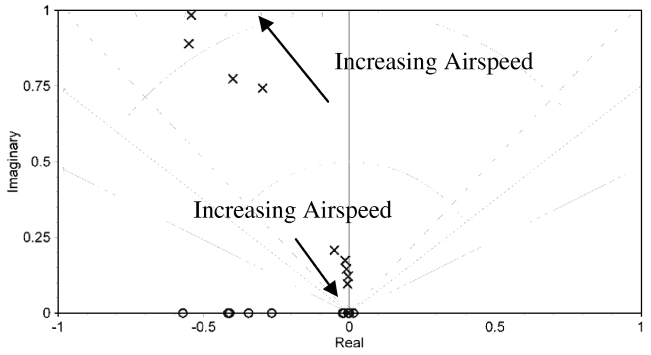

Fig. 1 Pole/zero migration with airspeed for low speed, high α trim cases.

Table 1 Rigid body longitudinal mode variation with airspeed

V, kt	$[\zeta_P, \omega_{nP}]$	$[\zeta_{SP}, \omega_{nSP}]$	$1/T_{\theta 1}$	$1/T_{\theta 2}$
110	[0.2392, 0.2140]	[0.3717, 0.80]	0.0020	0.2661
160	[0.0633, 0.1524]	[0.4753, 1.06]	0.0074	0.3925
250	[0.0636, 0.0967]	[0.5007, 1.44]	0.0188	0.5709
400	[0.1354, 0.0584]	[0.5497, 2.04]	0.0192	0.9211

II. Aircraft Model

The test vehicle used for the study is the longitudinal F-16 aircraft model based on NASA Langley Research Center wind tunnel tests [9]. The F-16 is a relaxed static stability aircraft, meaning that its bare airframe dynamics possess very lightly damped or unstable poles for most of the flight envelope. This problem tends to become complicated at higher angles of attack and lower speeds, which is an indicator of potential issues during control development. Nonminimum phase zeros are also present for some flight conditions, leading to a difficult control problem in certain corners of the flight envelope. The details of nonlinear modeling and simulations of the F-16 aircraft are presented in [10].

The nonlinear equations of motion for the aircraft can be linearized in pitch and represented in either state-space or transfer function form. To include high α trim conditions in the control design, an altitude of 12,000 ft was chosen as the baseline flight condition. This allows for a range of trim angles of attack from 1 to 30 degrees corresponding to a variation in trim airspeed of 110–400 kt from which flight conditions for control design and flight simulation were selected. Transfer functions for all of the chosen flight conditions corresponding to a 12,000 ft flight altitude were generated with pitch rate, pitch attitude, and angle of attack as outputs and the poles and zeros were plotted for each. Pole and zero migrations for very low speed (i.e., 110–160 kt), high α cases are shown in Fig. 1. The dynamics for the four flight conditions of interest are summarized in Table 1, where the subscripts P and SP denote phugoid and short period modes while $T_{\theta 1}$ and $T_{\theta 2}$ are the transfer function zeros. For a typical longitudinal transfer function, the phugoid pole is at a much lower frequency and more lightly damped than the short period pole. As seen in Fig. 1, the phugoid mode tends to migrate toward, but not cross into, the right half-plane as airspeed increases. There are also nonminimum phase zeros for the lower speed cases, though at 110 kt the $T_{\theta 1}$ zero is in the left half-plane.

The complete flight envelope studied in this research is shown in Fig. 2. Flight conditions near 200 kt can be defined as transitional; that is, they exist in a locus of high power, high α trim conditions below those that would be considered normal, level flight for the F-16. The analysis shows that it is only in these transitional cases that right half-plane phugoid poles exist. For both lower and higher speeds, the phugoid mode is lightly damped but still exhibits stable behavior. Because the phugoid mode is typically controlled by the pilot loop closure, the classical control design in the next section focuses on short period damping and frequency and uses the method established in [11].

III. Control Methods

This research sought to address the question of which control design methods are best suited to a high performance aircraft application. In this section, three different control methods, classical, H_∞, and LPV, are applied to the longitudinal F-16 aircraft model.

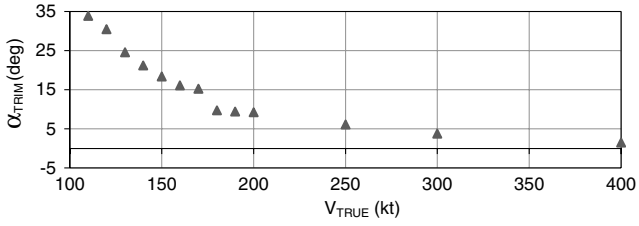

Fig. 2 Flight envelope trim conditions.

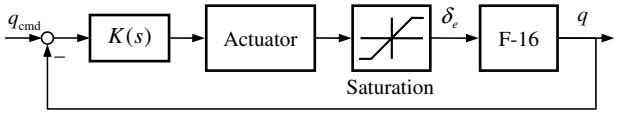

Fig. 3 PI control loop architecture.

The control objective is to track the command of the pitch rate. For all methods, the control design requirements are the same, i.e., to achieve good tracking performance with a fast speed of response, a small overshoot, and a small steady-state error. It should be pointed out that the design requirements are incorporated into different control methods in different ways.

A. Classical Control Design

The advantage of classical control design methods is simplicity. Many systems can be adequately compensated with first- or second-order controllers. It is desirable for the compensator design to be of lower order to keep complexity to a minimum while still providing adequate closed-loop control of the aircraft. Figure 3 shows the feedback control block diagram, where a 10 Hz critically damped second-order actuator model and ± 25 deg elevator position limit were added to more completely model the aircraft response to pitch rate commands. The actual F-16 actuator models are consistent with these assumptions.

For the current design, PI controller in the form of

$$K(s) = \frac{k_q}{s}\left(s + \frac{1}{T_q}\right) \tag{1}$$

is used to draw the short period dynamics toward a more desirable state and forces the phugoid dynamics into two real zeros through the placement of the compensator zero. The gain k_q is selected for each flight condition to provide a closed-loop short period mode with a damping ratio of 0.6–0.7 at a frequency of 4.0–5.0 rad/s, which provides a reasonably damped overshoot. Command overshoot is acceptable as it results in a highly responsive airplane while the relatively high bandwidth allows for pilots to compensate for the error generated with the pilot loop closure. The gain k_q is scheduled on airspeed between different flight conditions.

The $1/T_q$ compensator zero is placed above the rigid body dynamics but is located below the desired crossover frequency, giving it the desired k/s-like characteristic in the crossover region. The term "k/s-like" refers to the behavior of a response which exhibits the characteristics of a single integrator $1/s$ with a pure gain k. This is desirable as the pilot-vehicle crossover model states that an aircraft which exhibits this behavior is likely to require less pilot compensation and therefore induce less workload [12]. For the chosen flight envelope, the $1/T_q$ compensator zero is chosen to be 3.

Classical frequency domain methods were used to determine the open-loop stability margins and closed-loop short period damping and frequency for various values of k_q. As shown in Table 2, gain and phase margins are denoted as GM and PM, and ζ'_{SP} and $\omega'_{n\text{SP}}$ are closed-loop short period damping and frequency. It can be seen that stability margins are not of concern, as a surplus of phase margin is present and gain margin is much greater than the established minimum of 6 dB at the -180 deg phase crossover frequency. Gains are negative because a positive pitch rate command results in a negative elevator deflection.

Table 2 Open-loop short period stability margins and closed-loop short period dynamics

V, kt	k_q	PM, deg	GM, dB	$[\zeta'_{\text{SP}}, \omega'_{n\text{SP}}]$
110	−240	57.17	26.36	[0.61, 3.72]
160	−100	60.01	26.22	[0.64, 3.81]
250	−45	63.42	26.38	[0.66, 3.91]
400	−17	70.50	26.72	[0.68, 4.14]

B. H_∞ Control Design

An H_∞ control problem can be solved via either algebraic Riccati equations [13] or linear matrix inequalities [14] (LMIs). In this research, the LMI approach was used to derive an H_∞ controller for every flight condition shown in Fig. 2. A block diagram of the system interconnection for synthesizing the H_∞ controller is shown in Fig. 4. The F-16 linear plant dynamics contain five states and two control inputs for elevator and throttle. The outputs are aircraft velocity V, pitch rate q, and flight path angle γ. Weighting functions to simulate actuator dynamics and measurement noise are included, in addition to weighting functions designed to penalize the control effort and filter the error signal. For the current design, a dynamic output-feedback controller in the form of

$$\begin{bmatrix} \dot{x}_k \\ u \end{bmatrix} = \begin{bmatrix} A_k & B_k \\ C_k & D_k \end{bmatrix} \begin{bmatrix} x_k \\ y \end{bmatrix} \tag{2}$$

is derived using the linearized system dynamics for every trim condition in addition to the weighting functions, where x_k is the state of the controller.

To incorporate the design requirements, the H_∞ control design is formulated as a model-following problem. The ideal pitch rate response of the aircraft to a pitch rate command is chosen as

$$W_{\text{ideal}} = \frac{q_{\text{ideal}}}{q_{\text{cmd}}} = \frac{7.2^2}{s^2 + 2(0.8)(7.2)s + 7.2^2}$$

It should be mentioned that the same ideal command weighting function W_{ideal} is used for H_∞ control design at all selected flight conditions. To achieve a more satisfactory result for the entire flight envelope, the weighting function was tuned, which does not provide the exactly same amount damping and natural frequency as the classical controller at all flight conditions. The tracking error is defined as $q - q_{\text{ideal}}$. This error signal is allowed to be large for frequencies above the system bandwidth frequency and small for

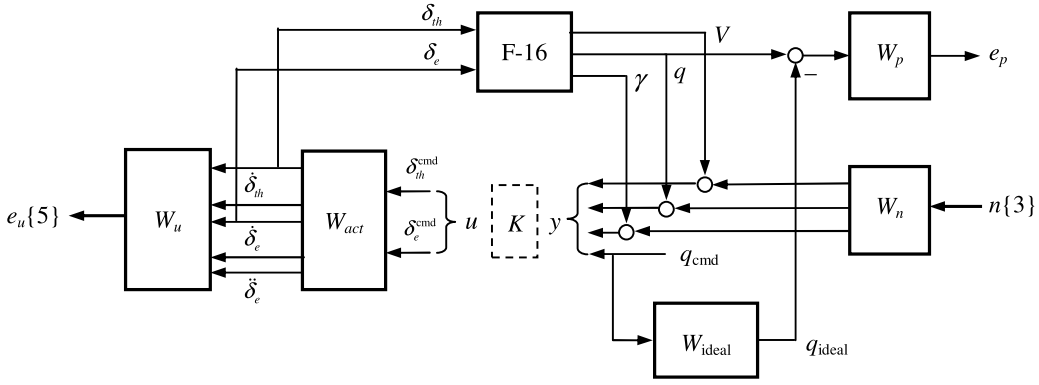

Fig. 4 Weighted open-loop interconnection for H_∞ control of F-16 aircraft.

frequencies where the system can track commands. This is accomplished through the lag-lead weighting filter W_p defined as

$$W_p = \frac{0.818s + 70.71}{s + 0.7071}$$

The dynamics of the actuators are modeled as a first-order transfer function

$$\frac{\delta_{\text{th}}}{\delta_{\text{th}}^{\text{cmd}}} = \frac{10}{s + 10}$$

for the throttle and a second-order transfer function

$$\frac{\delta_e}{\delta_e^{\text{cmd}}} = \frac{62.8^2}{s^2 + 2(0.7)(62.8) + 62.8^2}$$

for the elevator. Since the closed-loop performance objectives include penalties on the deflections and rates of both actuators as well as the acceleration of the elevator, the weighting function W_{act} created based on the previous two transfer functions has five outputs as shown in Fig. 4. These signals should remain reasonably small in the face of the exogenous signals, and they are weighted by W_u to give an actuator error vector e_u, where

$$W_u = \text{diag}\{0.1, 0.1, 0.1, 0.001, 0.0002\}$$

There are two sources of exogenous signals, sensor noise and pilot pitch rate command. The weighting function W_n is chosen as

$$W_n = \text{diag}\{0.8, 0.6, 0.1\}$$

which implies a measurement error in velocity of 0.8 ft/s, an error in pitch rate of 0.6 deg/s, and an error in flight path angle of 0.1 deg. The H_∞ control design is dealt with using the MATLAB Robust Control Toolbox [15].

C. LPV Control Design

LPV control theory is an extension of H_∞ control theory. The general framework used for LPV control design is shown in Fig. 5 with plant $P(\rho)$, controller $K(\rho)$, control inputs u, disturbance inputs w, controlled outputs z, and measured outputs y. The state-space data of the plant $P(\rho)$ depend continuously on a time-varying parameter $\rho(t)$, and the controller $K(\rho)$ is scheduled based on the varying parameter $\rho(t)$.

Consider an LPV plant $P(\rho)$ given by

$$\begin{bmatrix} \dot{x} \\ z \\ y \end{bmatrix} = \begin{bmatrix} A(\rho) & B_1(\rho) & B_2(\rho) \\ C_1(\rho) & D_{11}(\rho) & D_{12}(\rho) \\ C_2(\rho) & D_{21}(\rho) & D_{22}(\rho) \end{bmatrix} \begin{bmatrix} x \\ w \\ u \end{bmatrix} \tag{3}$$

where all matrix-valued state-space data have appropriate dimensions. The time-varying parameter $\rho(t)$ is assumed bounded. Similar to H_∞ control, we are interested in designing a dynamic output-feedback controller of the LPV form:

$$\begin{bmatrix} \dot{x}_k \\ u \end{bmatrix} = \begin{bmatrix} A_k(\rho) & B_k(\rho) \\ C_k(\rho) & D_k(\rho) \end{bmatrix} \begin{bmatrix} x_k \\ y \end{bmatrix} \tag{4}$$

If there exist positive definite matrices R and S such that the following LMIs

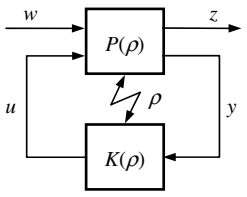

Fig. 5 General framework for LPV control design.

$$\begin{bmatrix} N_R(\rho) & 0 \\ 0 & I \end{bmatrix}^T \begin{bmatrix} A(\rho)R + RA^T(\rho) & RC_1^T(\rho) & B_1(\rho) \\ C_1(\rho)R & -\gamma I & D_{11}(\rho) \\ B_1^T(\rho) & D_{11}^T(\rho) & -\gamma I \end{bmatrix} \times \begin{bmatrix} N_R(\rho) & 0 \\ 0 & I \end{bmatrix} < 0$$

$$\begin{bmatrix} N_S(\rho) & 0 \\ 0 & I \end{bmatrix}^T \begin{bmatrix} A^T(\rho)S + SA(\rho) & SB_1(\rho) & C_1^T(\rho) \\ B_1^T(\rho)S & -\gamma I & D_{11}^T(\rho) \\ C_1(\rho) & D_{11}(\rho) & -\gamma I \end{bmatrix} \times \begin{bmatrix} N_S(\rho) & 0 \\ 0 & I \end{bmatrix} < 0 \qquad \begin{bmatrix} R & I \\ I & S \end{bmatrix} \geq 0 \tag{5}$$

are satisfied for all ρ, where $N_R(\rho)$ and $N_S(\rho)$ are matrices whose columns form bases of the null spaces of $[B_2^T(\rho) \quad D_{12}^T(\rho) \quad 0]$ and $[C_2(\rho) \quad D_{21}(\rho) \quad 0]$, then the closed-loop LPV system is internally stable, and simultaneously we have the H_∞ norm of the closed-loop system less than the parameter γ, i.e., $\|z\|_2 < \gamma\|w\|_2$.

The above LMIs in Eq. (5) are the synthesis conditions for the LPV control design, and the derivation is similar to that in [14]. The MATLAB Robust Control Toolbox offers tools to specify, manipulate, and numerically solve LMIs. The LMI solver *mincx* is used to find the solution of the LMIs for a minimum value of γ. After solving R, S, and γ, the LPV controller can be constructed using the following formula [16]:

$$\begin{aligned} A_k(\rho) &= -N^{-1}\{A^T(\rho) + S[A(\rho) + B_2(\rho)F(\rho) + L(\rho)C_2(\rho)]R \\ &\quad + \frac{1}{\gamma}S[B_1(\rho) + L(\rho)D_{21}(\rho)]B_1^T(\rho) \\ &\quad + \frac{1}{\gamma}C_1^T(\rho)[C_1(\rho) + D_{12}(\rho)F(\rho)]R\}M^{-T} \\ B_k(\rho) &= N^{-1}SL(\rho) \qquad C_k(\rho) = F(\rho)RM^{-T} \qquad D_k(\rho) = 0 \end{aligned} \tag{6}$$

where $N = S, M = S^{-1} - R$, and the matrix functions $F(\rho)$ and $L(\rho)$ are defined as

$$\begin{aligned} F(\rho) &= -(D_{12}^T(\rho)D_{12}(\rho))^{-1}[\gamma B_2^T(\rho)R^{-1} + D_{12}^T(\rho)C_1(\rho)] \\ L(\rho) &= -[\gamma S^{-1}C_2^T(\rho) + B_1(\rho)D_{21}^T(\rho)](D_{21}(\rho)D_{21}^T(\rho))^{-1} \end{aligned} \tag{7}$$

To improve the probability that a set of R and S matrices will be found and to improve the performance of the resulting controller $K(\rho)$, the matrix variables R and S are allowed to vary linearly with the scheduling parameter ρ such that

$$R(\rho) = R_0 + \rho R_1 \qquad S(\rho) = S_0 + \rho S_1 \tag{8}$$

This allows the controller constructed from $R(\rho)$ and $S(\rho)$ and derived from the complete set of LMIs more freedom to provide optimum performance for all operating conditions while still offering the benefit of a stability guarantee.

Different from the LMI formulation of H_∞ control, the state-space matrices of the plant for LPV control are continuous functions of the scheduling parameter ρ. Theoretically, the synthesis conditions in Eq. (5) must hold for any value of the scheduling parameter ρ in the allowable region, making it an infinitely LMI-constrained problem. In many practical problems, the parameter dependency is dealt with using the "gridding" approach. Assume that n discrete values of the scheduling parameter ρ are selected and are dense enough to represent the dynamics over the entire parameter region. The LMI problem for LPV control design can then be expressed as $3n$ LMIs. Whereas in H_∞ control a single operating condition is used to construct a single controller through an LMI minimization, the entire set of linear state-space models is used to construct a series of LMIs which are then minimized to find the matrices R and S used to construct the LPV controller $K(\rho)$. The state-space matrices of the controller also depend on the scheduling parameter ρ. The controller

resulting from the LPV control approach stabilizes the closed-loop system for all operating conditions in the allowable region.

For the current formulation, ρ is selected to be airspeed and the flight envelope is to be defined as shown in Fig. 2 where 14 distinct trim points between 110 and 400 kt are selected. The LPV control problem was set up identically to the H_∞ problem, and the design requirements are incorporated into LPV control in the same way as the previously described H_∞ control. The weighted interconnection block diagram is shown in Fig. 4 and described in Sec. III.B. The plant dynamics, weighting functions, and LMI formulations are all identical between the two; the only difference being the number of LMIs.

In regard to control design effort, on the one hand, classical controllers are of lower order and easy to design. While robust H_∞ and LPV controllers are of higher order. In particular, the robust control design significantly depends on weighting functions, which are usually selected based on empirical assumption. This makes the control design process complicated. On the other hand, classical and H_∞ controllers are purely linear controllers, and a family of point controllers must be designed throughout the operation region. It will be a time-consuming and tedious process for a wide flight envelope with significantly varying flight conditions. However, the LPV control method avoids this issue and generates one controller $K(\rho)$ based on all flight conditions.

IV. Desktop Simulation Results and Analysis

After three flight controllers were developed for the F-16 VISTA aircraft using classical control design method in addition to H_∞ and LPV robust design methods, desktop analysis and simulation were used to assess and compare the performance of each controller.

A. Implementation Considerations

Of the many differences in the three control design methodologies to be compared, there exist advantages and disadvantages for each in regard to piloted simulation. First and foremost is the implementation advantage of the classical controller over the two robust controllers. The classical controller is first order with a single scheduled gain and can be easily implemented in a simulator. However, the H_∞ and LPV controllers are of higher order and much more computationally intensive. In addition, the classical and H_∞ controllers are scheduled using linear interpolation and can be easily computed in real time. But the LPV controller is parameter-varying in simulation and theoretically should be determined online following Eqs. (6) and (7). To reduce real-time computation effort, usually a relatively coarse gridding parameter space is used for synthesis and then control gains are constructed off-line at finer gridding points and saved as look-up tables. They are interpolated online according to the real-time parameter values.

Table 3 Closed-loop performance metrics for various designs

V, kt	*Classical*		H_∞		*LPV*	
	ω_{BW}, rad/s	τ_p, s	ω_{BW}, rad/s	τ_p, s	ω_{BW}, rad/s	τ_p, s
110	3.78	0.0192	2.39	0.190	3.00	0.137
160	3.89	0.0191	2.83	0.155	3.29	0.093
250	3.99	0.0190	3.05	0.126	3.42	0.045
400	4.18	0.0190	3.17	0.098	3.46	0.038

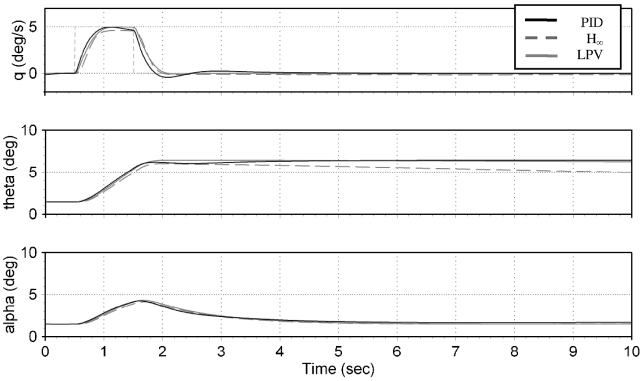

Fig. 7 Comparison of responses to pulse input, 400kt.

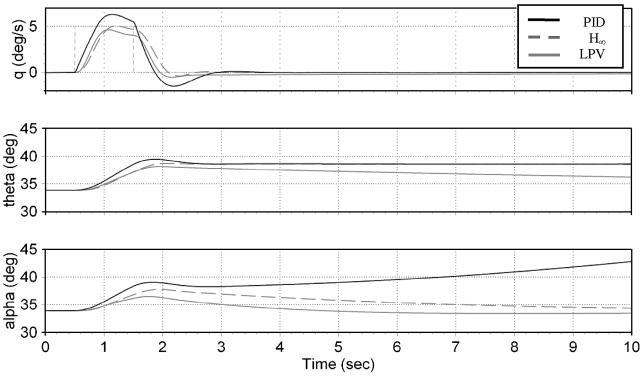

Fig. 8 Comparison of responses to pulse input, 110 kt.

B. Performance Metrics

Performance metrics are designed to be measures of system performance, which predict closed-loop flying qualities under piloted control. Listed in [17] are six different criteria for the prediction of pilot opinion, but because the simulation will consist of up-and-away tasks that will likely require high pilot gain and tight closed-loop control, the bandwidth/phase delay criterion is the primary figure of merit in the comparison of the closed-loop system characteristics. Table 3 and Fig. 6 give a summary of the closed-loop performance metrics, including bandwidth frequency ω_{BW} and phase delay τ_p, for the three designs at four flight conditions of interest. In Fig. 6, the data in Table 3 is overlaid onto the bandwidth/phase delay criterion described in [17]. The colored regions represent the level 1 (bottom right corner), 2 (middle), and 3 (upper left corner) handling qualities regions.

Some trends which were observed in the data:

1) Bandwidth increases and phase delay decreases with increasing airspeed.

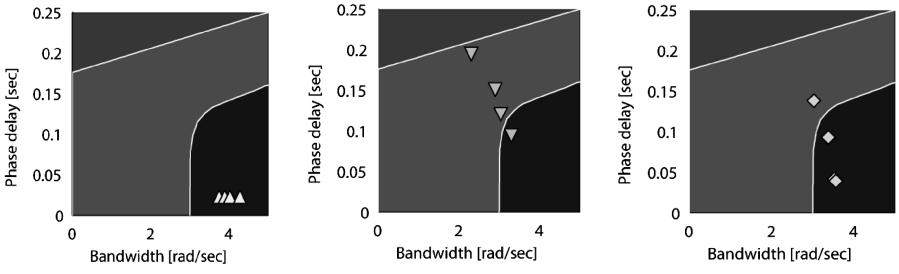

a) Classical **b) H_∞** **c) LPV**

Fig. 6 Closed-loop bandwidth and phase delay for various flight controllers.

2) Bandwidth varies minimally across the flight envelope for all three designs.

3) Phase delay is almost invariant for the PID controller and is significantly lower than either of the robust controllers.

4) Bandwidth and phase delay for the H_∞ controller are considered deficient for all flight speeds when compared with the other designs.

C. Simulation Results

The resulting three control systems were implemented in Simulink. Overall, they all achieved the desired tracking performance. Figures 7 and 8 show the responses to a pulse rate command of 5 deg/s for 400 and 110 kt trim cases for brevity. It was observed that the performance is nearly identical for higher airspeeds where trim angle of attack is near zero. However, for lower airspeeds where trim angle of attack is large, tracking performance varies for different control methods.

As shown in Fig. 8, the classical controller exhibited more overshoot than either H_∞ or LPV control methods. This is to be expected as the damping requirement set for both H_∞ and LPV controllers are slightly higher than that for the classical control at the airspeed of 110 kt. However, for the current application in which the controller is meant to stabilize and control a highly agile fighter-type aircraft, damping out overshoot comes with the penalty of lower bandwidth and a much slower response. Having an acceptable amount of bandwidth can be seen as beneficial in Fig. 8, as it induces lead which hastens the rate response and provides a faster attitude change with minimal overshoot for the response using the classical controller. The H_∞ and LPV controllers show a much larger amount of phase delay and an attitude response that lags behind that of the classical controller.

Another observation made in the analysis of the responses is that of a steady-state pitch rate error. The performance weighting function W_p in the robust controller formulation used to develop the H_∞ and LPV controllers allows for a small amount of steady-state error, which in the case of attitude command-type systems is acceptable and has little effect on pilot ratings, but for the rate command system currently implemented the associated pitch attitude roll off may result in degraded flying qualities.

V. Piloted Simulation Test Plan

The primary objectives of the piloted simulation study in this research are as follows:

1) Investigate the differences in closed-loop bandwidth and phase delay for all controller designs.

2) Attempt to expose any stability deficiencies present in the defined flight envelope.

3) Evaluate tracking performance for various trim conditions and airspeeds.

4) Track pilot workload and input spectra to provide an additional performance assessment metric.

A. Flight Simulator

The piloted simulation was conducted using the System Technology, Inc., (STI), fixed base simulator. Figure 9 shows the key hardware system components to the STI pilot-in-the-loop flight simulator [18].

The simulator is a Win32 console application designed to interface with MATLAB for data input and output. A dynamically linked library was developed to simulate the dynamic equations of motion for the F-16 aircraft based on the model provided by Dr. E. A. Morelli [10] which accepts stick displacements as inputs and sends vehicle rates and attitudes as outputs. The current PC-based simulator features 1) linear airframe equations of motion; 2) software rate limits, surface position limits, and actuator models; 3) data recording of unlimited output states; 4) vehicle dynamics that update at 120 Hz and graphics that update at a minimum of 30 Hz; and 5) texture-mapped PC graphics with a superimposed head-up display that supports pitch and roll axis tracking tasks.

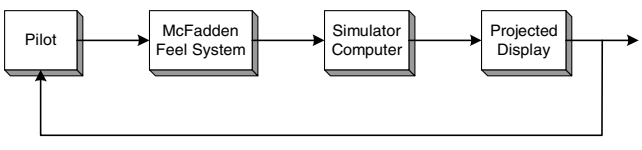

Fig. 9 Pilot-in-the-loop simulator elements.

Table 4 Trim conditions for piloted simulation

V, kt	α, deg	δ_e, deg
110	33.87	−10.49
160	16.12	−4.23
250	6.09	−2.95
400	1.50	−1.75

B. Flight Conditions

The flight envelope defined in this study focuses on low speed, high angle of attack trim conditions for a 20,500 lb aircraft with a longitudinal center of gravity location of 30% of mean aerodynamic chord. For completeness, moderate speed trim conditions are included to investigate the handling qualities at more conventional operating points.

Rather than conduct a simulation run for each flight condition in the defined envelope, the simulation test will focus on a few distinct trim cases which together will adequately represent the entire envelope. Shown in Table 4, the selected trim conditions span the entire range of trim airspeeds and include two intermediate flight conditions which fill in the remainder of the envelope. A very low speed, high angle of attack case will be examined as the elevator deflection required for trim is large and encountering surface saturations is likely. This is a case of interest as encountering rate or travel limits often affects task performance and may even lead to PIO. Tasks will be flown for each controller at each flight condition in order to collect enough data for a detailed analysis.

C. Sum-of-Sines Tracking Task

The STI flight simulator was designed to simulate aircraft in up-and-away flight. Because the current work has focused on low to moderately-low airspeeds and ease of implementation is of importance, the evaluation will focus on a sum-of-sines (SOS) tracking task in the longitudinal axis only for the selected flight conditions. This will provide adequate simulation test data to perform a handling qualities assessment across the entire flight envelope for each controller and investigate pilot behavior while keeping required simulation time to a minimum.

The SOS task is a valuable and robust form of computer-generated command that can provide valuable data used to extract information about the pilot-vehicle system [19]. Note that the signal displayed to the pilot is the tracking error, not the command signal. In pitch, this means that $\theta_{\text{display}} = \theta_c - \theta$, where θ_c is the command from the SOS waves and θ is airplane attitude, making the task compensatory so that the pilot compensates for changes and does not pursue an attitude command.

Table 5 SOS command signal for pitch

Sine wave number	*Pitch attitude*		
	A_i, deg	Number of cycles	ω_i, rad/s
1	−1	2	0.19947
2	1	5	0.49867
3	1	9	0.8976
4	0.5	14	1.39626
5	−0.2	24	2.39359
6	0.2	42	4.18879
7	−0.08	90	8.97597

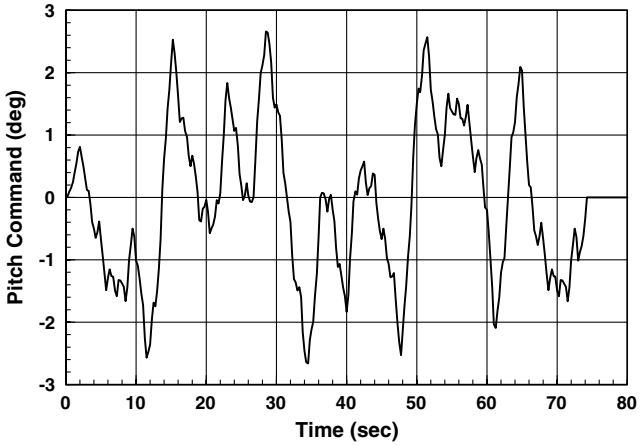

Fig. 10 Example pitch axis SOS command signal.

The form of the SOS command is as follows:

$$\theta_c = \sum_{i=1}^{n} A_i \sin(\omega_i t + \phi_i) \tag{9}$$

The forcing functions used are given in Table 5, taken from [20]. Figure 10 shows a time history of the pitch command signal for reference. The task time is 74.25 s, consisting of 10 s of warm-up (nonscored time), 63 s of tracking for scoring, and 1.25 s of cool-down (nonscored time). All sine waves complete an integer number of cycles in 63 s, as listed in Table 5. Sine wave frequency, ω_i (in rad/s), is computed from the scoring time, t_s, and number of cycles of each sine wave, N_i, as follows:

$$\omega_i = \frac{2\pi N_i}{t_s} \tag{10}$$

More general guidelines for the selection of the forcing functions can be found in [19].

Evaluation pilots will aggressively track the displayed signal and attempt to keep errors within the specified tolerances. Desired and adequate performance limits are expressed in terms of milliradians (mils) of tracking error on the display. The desired performance criteria is ± 10 mils in pitch 50% of the simulation time and the adequate performance criterion is ± 20 mils in pitch 50% of the simulation time. These requirements are based on [20] but adjusted to be double as the work documented in [19] showed these limits to be too strict for pilots to meet.

D. Evaluation Procedure

The piloted simulation will serve as a handling qualities investigation of the performance of three independently-designed controllers. The procedures for the test will be as follows:

1) Evaluation pilots will be given a chance to familiarize with the simulator through several practice runs. Each flight condition will be presented to the pilot for familiarization with the task and vehicle behavior at that airspeed.

2) Formal evaluations will begin with the classical controller for the high speed (400 kt) trim case. The pilot will be asked to perform the evaluation task as many times as necessary for this controller and flight condition before providing pilot comments and ratings.

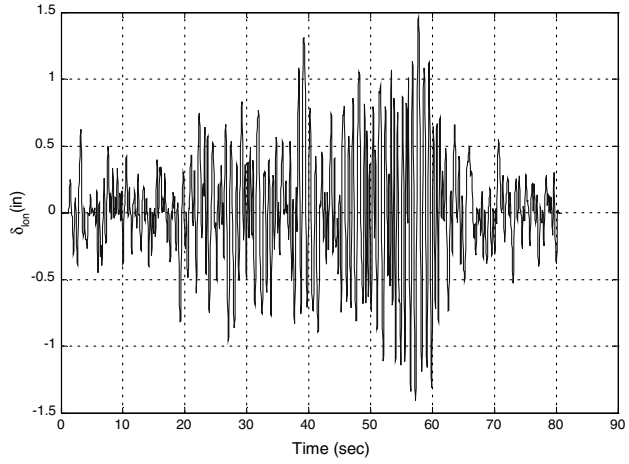

a) Pilot 1 stick input

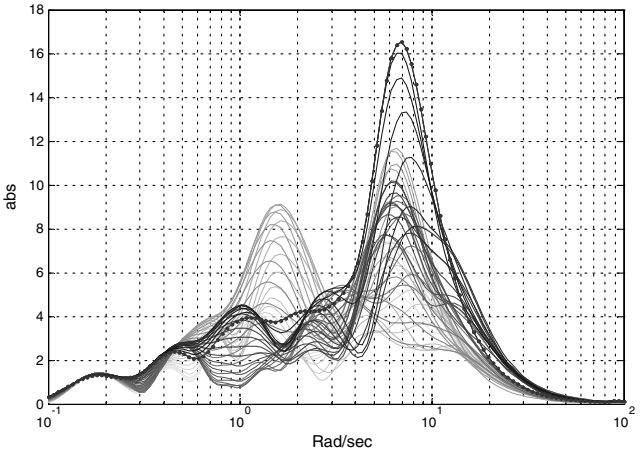

b) Pilot 1 scalogram: t = 28.5 – 58.5 seconds

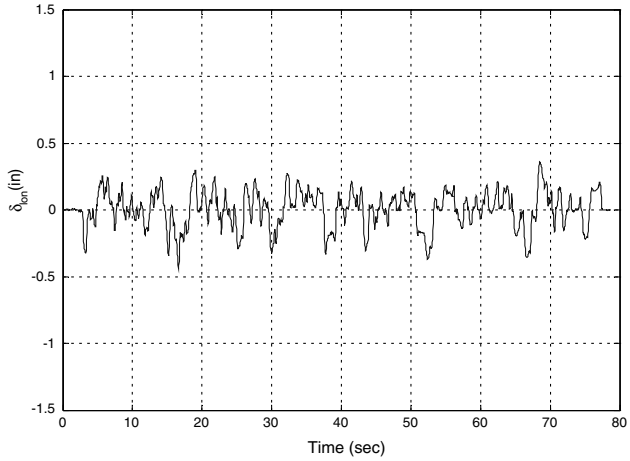

c) Pilot 2 stick input

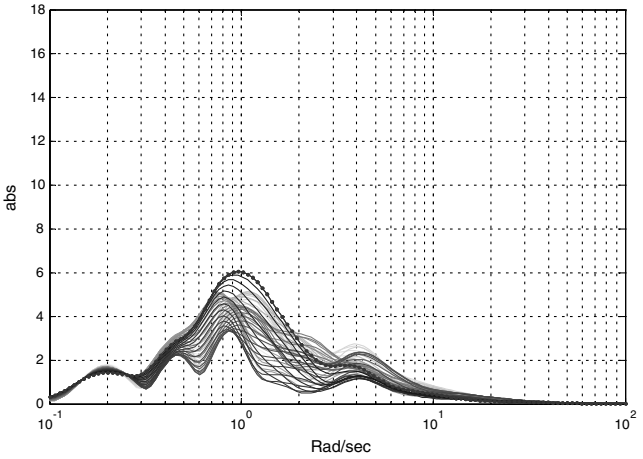

d) Pilot 2 scalogram: t = 22.4 – 52.4 seconds

Fig. 11 Time histories and scalograms for stick input, PID controller at 250 kt.

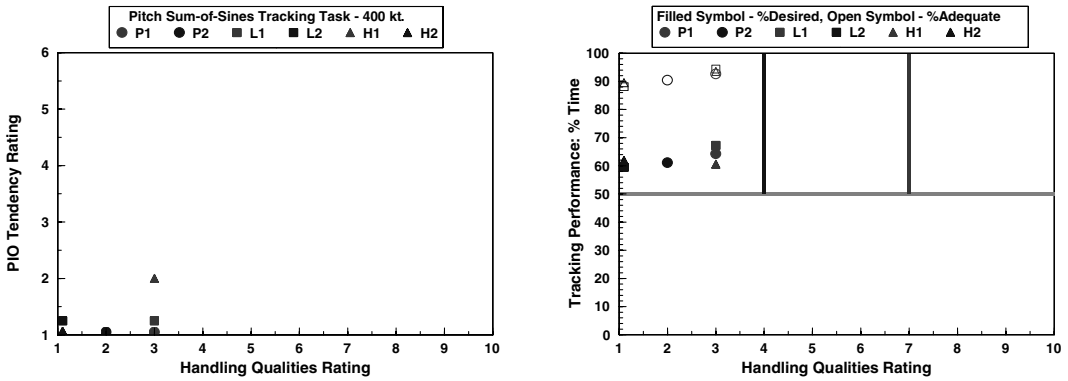

Fig. 12 Pilot ratings and tracking performance, 400 kt flight condition.

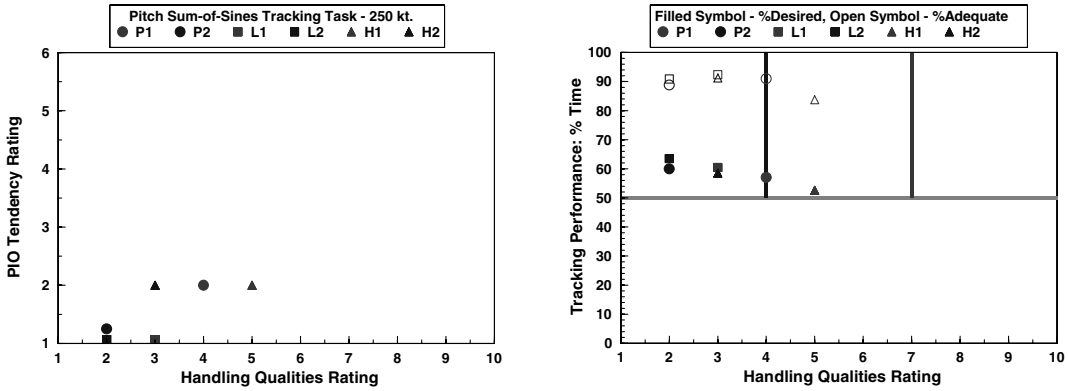

Fig. 13 Pilot ratings and tracking performance, 250 kt flight condition.

3) Cooper-Harper handling qualities ratings (HQRs) [21] and PIO tendency ratings [21,22] will be collected. Evaluation pilots will be strongly encouraged to talk their way through the rating scale decision trees as a means of extracting additional commentary.

4) Upon completion of the evaluation task and pilot ratings for the classically-designed controller, the scheduled H_∞ controller will be flown and evaluated, followed by the LPV controller for the 400 kt trim case.

5) The evaluation procedure described above will be repeated for 250, 160, and 110 kt trim cases.

6) A detailed run log will be recorded along with all pilot comments and ratings. Time history data will be saved in MATLAB format for future analysis.

VI. Piloted Simulation Test Results and Analysis

The flight simulation test was performed between 23 July 2009 and 5 August 2009 on the STI fixed base simulator in Hawthorne, California.

A. Pilot Technique and Rating Philosophy

Two pilots participated in the gathering of test data. Pilot 1 is a pilot and handling qualities engineer who has extensive experience with the SOS tracking task as well as conducting flight tests and simulation studies. Pilot 2 is also a pilot familiar with the SOS tracking task, holds a Ph.D. in Aerospace Engineering and is actively serving in the Navy reserve. The two pilots had distinct differences in technique as well as rating philosophy.

Pilot 1 approached SOS tracking as a task in which error was to be minimized, while pilot 2 sought only to keep pitch position error within desired and adequate error limits. As a result, pilot 1 was much more aggressive in his technique and applied much more energy to his input. Figure 11 shows an example pilot stick input for the entire task accompanied by a time-varying scalogram showing the input energy for a 30 s slice of each run. In the scalograms shown in Fig. 11b and 11d, the dark line with dots denotes the most recent estimate while the gray lines get increasingly light as time marches backward. As shown in Fig. 11, the most apparent distinction is the magnitude in which pilot 1 controls in comparison to pilot 2. Pilot 1 is

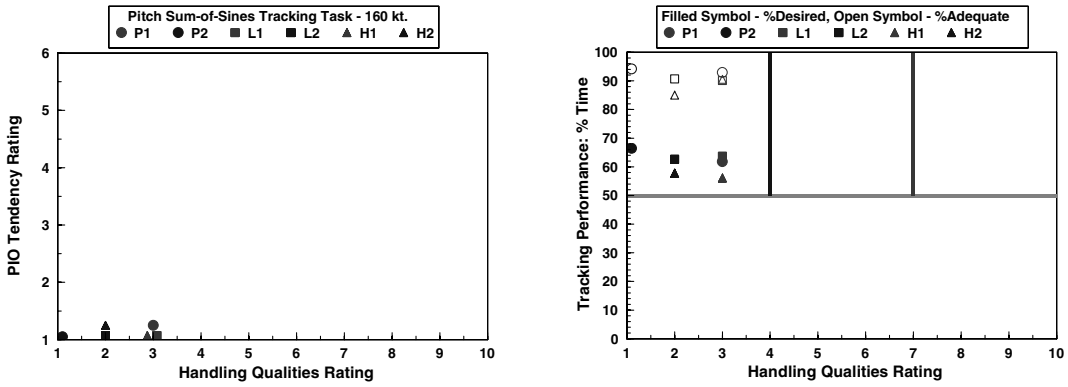

Fig. 14 Pilot ratings and tracking performance, 160 kt flight condition.

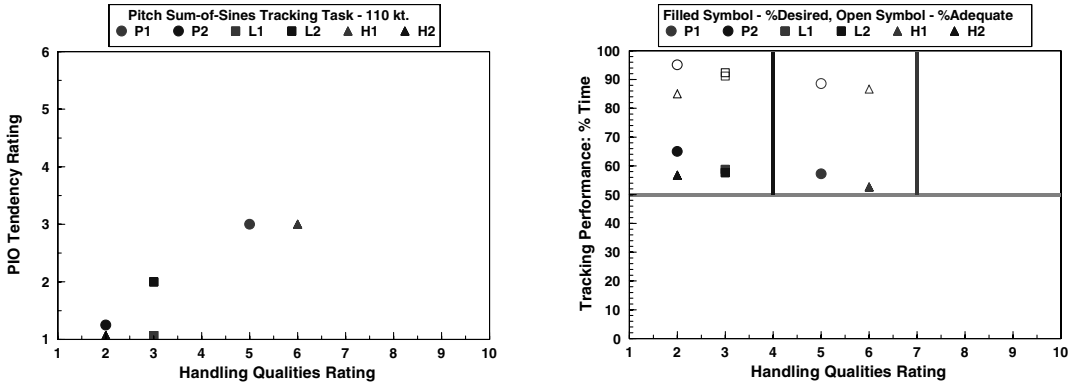

Fig. 15 Pilot ratings and tracking performance, 110 kt flight condition.

much more aggressive with his inputs, indicating an attempt at tighter tracking and reflecting the mentality that the goal of the task is to zero out any position errors. Pilot 2 uses much less input and changes input direction much less abruptly, indicating his tendency to keep error within performance limits and not to negate it completely. An examination of the scalograms gives additional insight into pilot technique and behavior in performance of the SOS task. Pilot 2 concentrates his inputs in the 0.5–3 rad/s frequency range with a magnitude peak occurring at 1 rad/s. Pilot 1 has a similar magnitude peak at about 1.5 rad/s, but also has a much larger magnitude peak at 8 rad/s. This correlates with the observations made previously in reference to the time history data that pilot 1 is controlling much more aggressively with both higher amplitude and frequency than pilot 2. More details on how to use wavelet transforms to obtain scalograms for detecting changes in fight control signals can be found in [23].

This difference in pilot technique is likely to become a factor in controller assessment as one of the main observations from the desktop analysis was that controller performance is very similar for higher airspeed flight conditions in which elevator saturations were not encountered. Aggressive pilot technique is likely to uncover these nonlinearities in the system and expose the pilot to any weaknesses in controller robustness while passive pilot technique is not. It is possible that the more passive pilot 2 may never encounter any elevator saturation limits due to his lack of command energy and ratings for these flight conditions will not reflect controller robustness to nonlinear phenomena.

The two pilots also varied significantly in rating philosophy. Pilot 1 stated in his pretest briefing that the best rating any configuration can receive for the SOS task is a HQR of 3 due to the inherent nature of the task. Pilot 2 was of the opinion that a perfectly-performing aircraft should always receive an HQR of 1 regardless of the task being performed. For this reason, pilot 2 rated well-performing controller-vehicle configurations 1 s and 2 s while pilot 1 rated well-performing configurations a 3. The purpose of the current work is to compare the performance and robustness of the three controllers against each other, not to compare the opinions of the two pilots for the same controller. Pilot ratings will be considered, but only in reference to handling qualities levels and not absolute ratings when compared between the two pilots. Absolute ratings will still be used to compare controllers, but for each pilot separately.

B. Handling Qualities Ratings and Comments

The pilot ratings for each of the 4 flight conditions considered as part of this study are given in Figs. 12–15. The configurations were flown "blind" in order to keep the pilot from rating based on direct comparison with the previous run.

In Figs. 12–15, the plots on the left show PIO tendency rating (PIOR) versus HQR, while the plots on the right show tracking performance presented as percent of task time versus HQR. Lighter markers indicate ratings and performance for pilot 1 while darker markers indicate ratings and performance for pilot 2. The legend distinguishes between controllers and pilots through symbol names according to the following convention: P1–PID controller/pilot 1, P2–PID controller/pilot 2, L1–LPV controller/pilot 1, L2–LPV controller/pilot 2, $H1$–H_∞ controller/pilot1, $H2$–H_∞ controller/pilot 2. The tracking performance plots show both desired and adequate performance, with desired performance shown as a closed symbol and adequate performance shown as the open version of the same symbol.

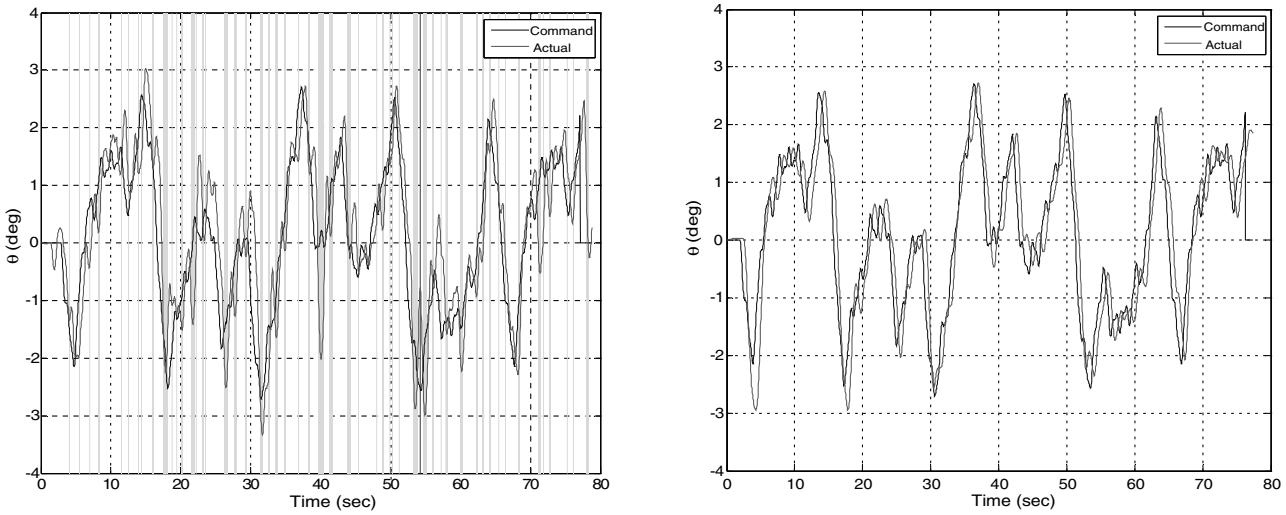

a) Pilot 1 – Lower limit: 17.57% of task time **b) Pilot 2 – No saturation encountered**

Fig. 16 Elevator saturation encountered during SOS tracking, PID controller at 110 kt.

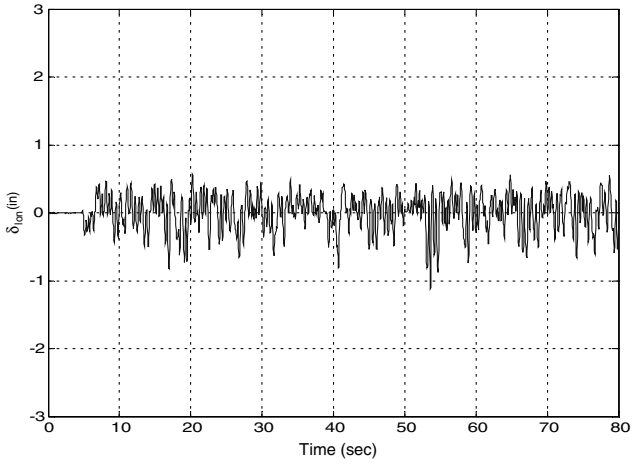

a) Compensatory tracking stick activity

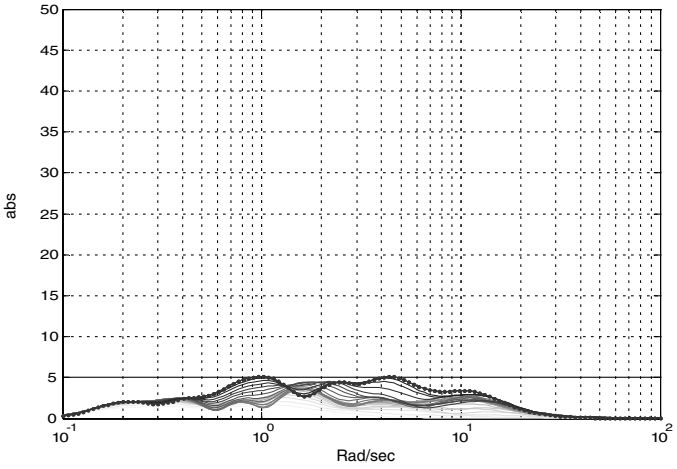

b) Scalogram

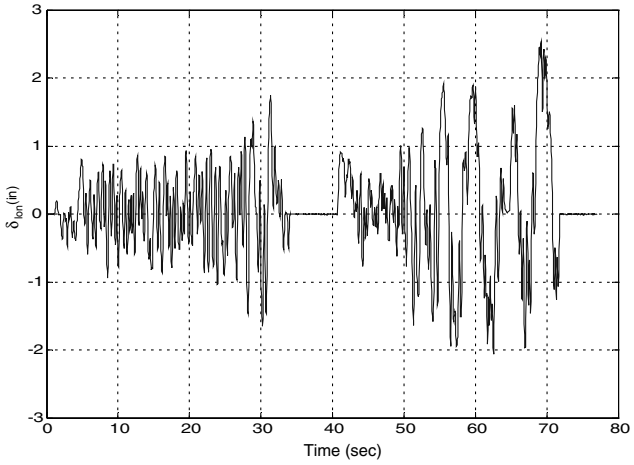

c) Aggressive tracking stick activity

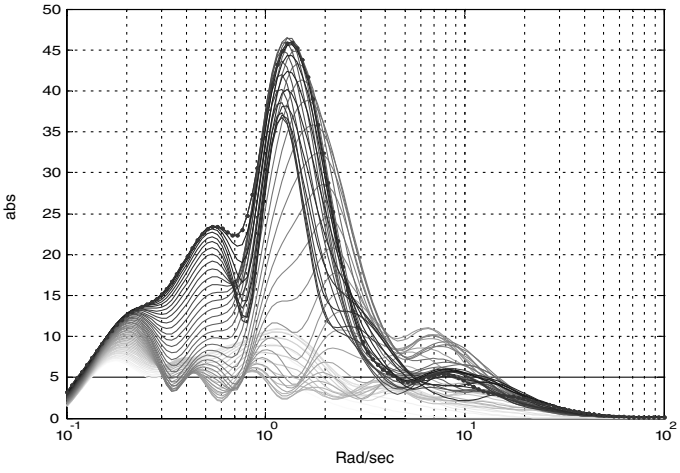

d) Scalogram

Fig. 17 Comparison of compensatory and aggressive tracking runs, H_∞ controller/110 kt.

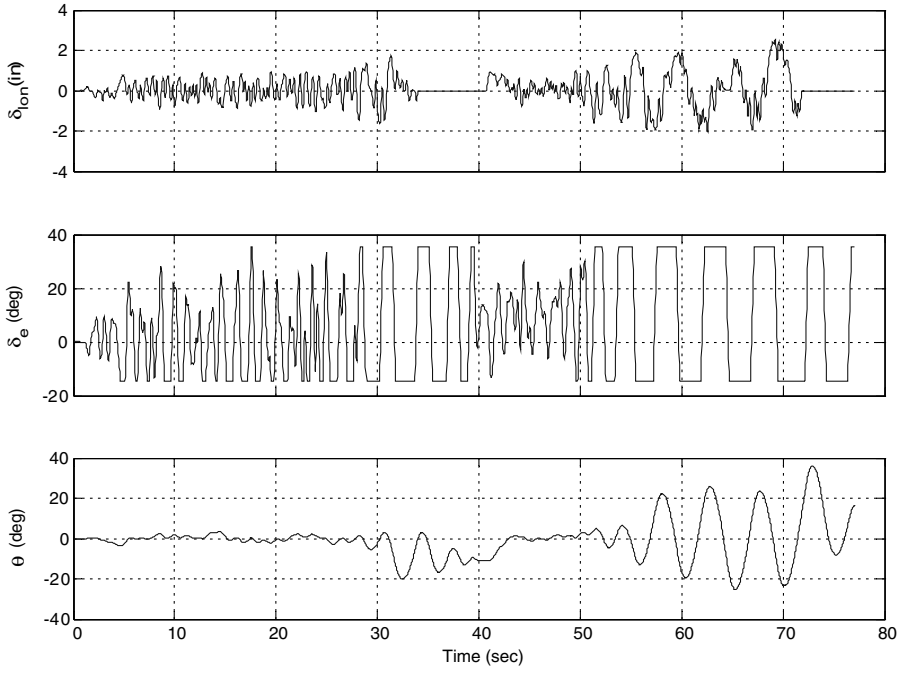

Fig. 18 Divergent PIO encountered during aggressive tracking, H_∞ controller/110 kt.

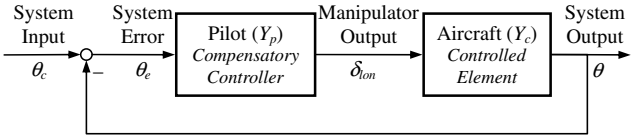

Fig. 19 Compensatory control scenario.

Focusing on the 110 kt flight condition shown in Fig. 15, pilot 2 rated all of the configurations as level 1 and had no problems achieving desired performance with all of the controllers. Pilot 1, however, gave level 2 ratings and had more difficulty achieving desired performance, though he was still able to do so through pilot compensation. This is evidenced by the observation that HQR and PIOR fell to level 2 while performance remained largely the same, indicating that pilot compensation and increased workload are to blame for the lower HQRs.

The differences in pilot opinion for this flight condition can be largely attributed to pilot technique. Whereas pilot 1 routinely encountered the elevator saturation limits at 110 kt, pilot 2 did not encounter limits during any of the evaluations. Figure 16 gives pitch attitude time histories for both pilots in their evaluation of the PID controller at 110 kt. In addition to the actual aircraft attitude, the command signal is shown for comparison. In Fig. 16, regions of saturation are shown highlighted in gray. Figure 16a shows that pilot 1 spends a considerable amount of task time on the lower saturation limit while Fig. 16b shows that pilot 2 does not encounter a saturation limit during his evaluation. Examination of the task performance data shows that pilot 2 was able to achieve desired performance for 65% of the task while pilot 1 was only able to achieve desired performance for 57.2% of the total task time. This data supports the conclusion that encountering the elevator saturation limit has an effect on task performance and the previously discussed conclusion that aggressive pilot technique is tied to this phenomenon. This is also reflected in the ratings given by both pilots in Fig. 15.

Based on the comments offered by pilot 1, it was noted that pilot 1 had difficulty distinguishing between controllers at higher airspeeds but noticed significant differences at lower airspeeds where elevator saturation is an issue for more aggressive pilot technique. This corresponds to the handling qualities and PIO ratings given by pilot 1 for the various configurations. As expected, the 110 kt case received the worst ratings from pilot 1 as encountering the elevator position limits affected his ability to perform the task. The exception for this flight condition was the LPV controller, which received a level 1 HQR and showed no tendency to induce pitch bobble or PIO. This controller showed comparable performance at higher airspeeds but for those flight conditions in which the other controllers showed unsatisfactory characteristics, it provided adequate stability and performance and no tendency to induce undesirable motion.

It should be noted that aggressive tracking or other high gain tasks are not uncommon for the F-16 aircraft considered in this study. Thus, pilot 1 participated in additional evaluation runs in which he attempted to force tracking error to zero through very aggressive technique. The 110 kt. case, of interest due to its exposure to elevator

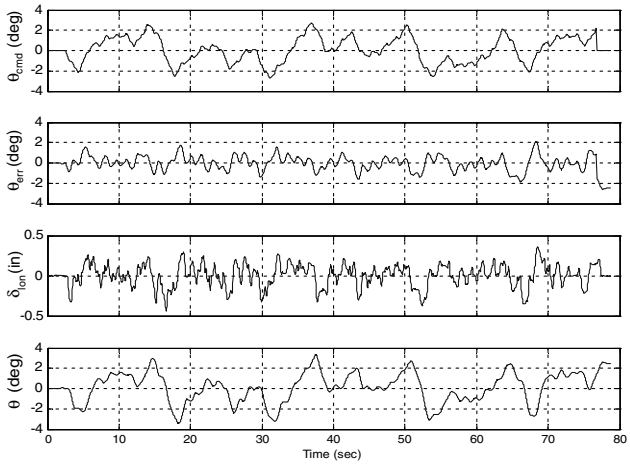

a) PID – HQR 2/PIOR 1

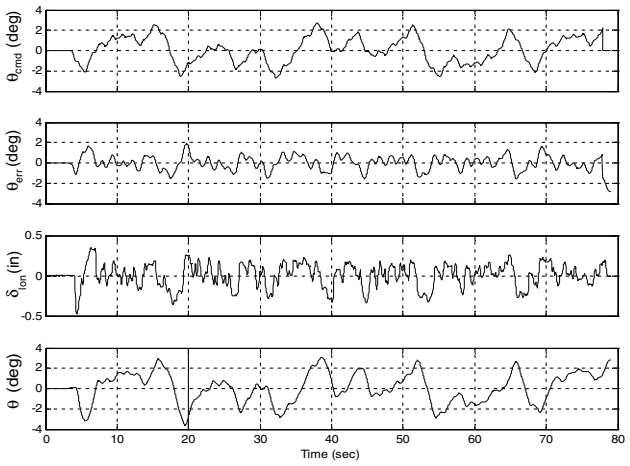

b) H_∞– HQR 3/PIOR 2

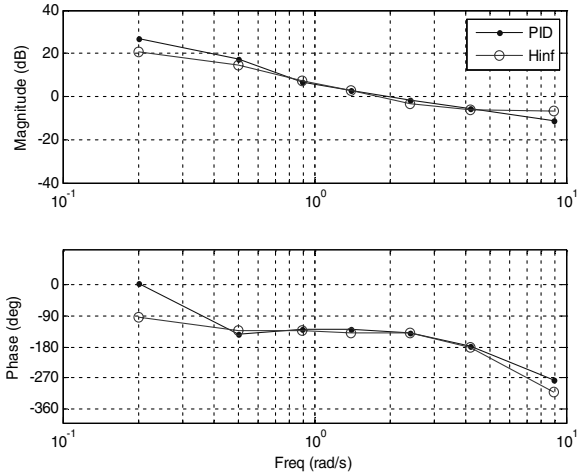

c) Pilot-vehicle system describing function (θ/θ_e)

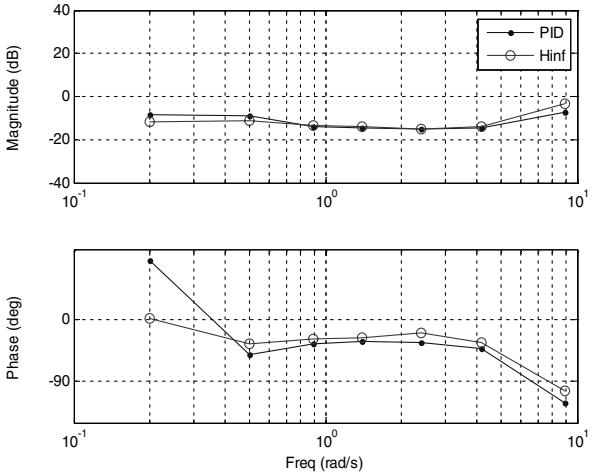

d) Pilot describing function (δ_{lon}/θ_e)

Fig. 20 Pilot-vehicle system describing function variation amongst controllers, pilot 2/250 kt.

Table 6 Pilot-vehicle system metrics, pilot 2/250 kt

Controller	ω_c, rad/s	τ_e, s	PM, deg
PID	1.93	0.406	45.14
H_∞	1.79	0.483	40.55

saturation, shows a profound change in pilot assessment for different controllers. Both the PID and H_∞ controllers experienced divergent PIOs where the pilot had to completely back out of the loop to regain control. The LPV controller fared much better, being degraded from level 1 to level 2 but not experiencing any divergent PIOs for aggressive maneuvers. As an example, shown in Fig. 17 are time histories and input scalograms for the compensatory tracking run as well as the aggressive tracking run for the H_∞ controller which resulted in a divergent PIO such as the one shown in Fig. 18.

C. Pilot-Vehicle Describing Functions

Also, the pilot-vehicle system metrics [24,25] have been computed and used as a supplement to the quantitative analysis data. A block diagram for the compensatory control scenario is shown in Fig. 19, where Y_p is the pilot describing function and Y_c is the vehicle describing function. The pilot controls the system output, θ, in response to the displayed pilot-vehicle system error, θ_e. With a known input function θ_c, the pilot and pilot-vehicle describing functions can be derived from the tracking task data and are of particular importance as they can be used to directly compare pilot behavior for the three controllers tested and determine if increased pilot compensation or workload is a factor in the degradation of ratings.

Time histories were created for the 4 signals in Fig. 19: θ_c, θ_e, δ_{lon}, and θ. As an example, Fig. 20 shows the pilot and pilot-vehicle describing function Bode plots for pilot 2's evaluation of the PID and H_∞ controllers at 250 kt, and the corresponding pilot-vehicle system metrics are given in Table 6. ω_c is the crossover frequency of the pilot-vehicle describing function at which the Bode magnitude plot crosses the 0 dB line. PM is the phase margin of the pilot-vehicle function. τ_e is the effective time delay and can be approximated as

$$\tau_e = \frac{\frac{\pi}{2} - \text{PM}}{\omega_c} \tag{11}$$

It is known that the crossover frequency of the pilot-vehicle system decreases with increased pilot compensation. The data shown in Table 6 and shown graphically in Fig. 20c indicate a higher level of pilot compensation for the H_∞ control. In addition, there is additional effective delay present and a decreased amount of phase margin, both of which also indicate an increase in pilot compensation for this configuration. The pilot describing function shown in Fig. 20d also leads to this conclusion, as the pilot is controlling with an additional amount of phase lead in an attempt to recover phase margin and to provide the additional compensation required for desired task performance. Though both configurations showed comparable performance, the H_∞ controller likely received lower ratings due to the higher pilot workload required.

VII. Conclusions

In this paper, three different control methods, classical, H_∞, and LPV, are assessed and compared through desktop analysis and piloted simulation. The results of the piloted simulation study clearly show that for higher airspeed flight conditions, there are no noticeable differences in the three controllers tested. This is in accordance with the findings of the desktop analysis and simulation, as it predicted similar flying qualities for the 400 kt flight condition. At lower airspeeds, however, both the desktop and pilot simulation results show that the controllers present distinguishable characteristics. It was found in the preliminary desktop analysis and simulation that the classically-designed controller held an advantage at very low airspeeds. But this was refuted in the piloted simulation study, which proved that the LPV controller was superior to both the classically-designed and H_∞ controllers in the presence of nonlinearities such as elevator saturation. Without introducing additional control approaches to handle saturation and without considering control design and implementation effort, it is concluded that the LPV control design technique is best suited for the fight-type aircraft studied in this current work. Classical control method is still attractive due to its simplicity and acceptable performance, and H_∞ control method is the worst one of the three. To obtain more statistically based results, more representative pilots will be used in the future to perform flight simulation and evaluate handling qualities.

Acknowledgments

The authors would like to thank Dave Klyde, Chi-Ying Liang, and Ed Bachelder at STI and Dave Mitchell at Hoh Aeronautics, Inc., for their help and guidance in this research effort.

References

[1] Balas, G. J., "Flight Control Law Design: An Industry Perspective," *European Journal of Control*, Vol. 9, Nos. 2–3, 2003, pp. 207–226. doi:10.3166/ejc.9.207-226

[2] Chiang, R. Y., Safonov, M. G., Haiges, K. R., Madden, K. P., and Tekawy, J. A., "A Fixed H_∞ Controller for a Supermaneuverable Fighter Performing a Herbst Maneuver," *Automatica*, Vol. 29, No. 1, 1993, pp. 111–127. doi:10.1016/0005-1098(93)90176-T

[3] Buffington, J. M., Sparks, A. G., and Banda, S. S., "Robust Longitudinal Axis Flight Control for an Aircraft with Thrust Vectoring," *Automatica*, Vol. 30, No. 10, 1994, pp. 1527–1540. doi:10.1016/0005-1098(94)90093-0

[4] Spillman, M. S., "Robust Longitudinal Flight Control Design Using Linear Parameter-Varying Feedback," *Journal of Guidance, Control, and Dynamics*, Vol. 23, No. 1, 2000, pp. 101–108. doi:10.2514/2.4492

[5] Lu, B., Wu, F., and Kim, S., "Switching LPV Control of an F-16 Aircraft via Controller State Reset," *IEEE Transactions on Control Systems Technology*, Vol. 14, No. 2, 2006, pp. 267–277. doi:10.1109/TCST.2005.863656

[6] Lu, B., and Wu, F., "Probabilistic Robust Linear Parameter-Varying Control of an F-16 Aircraft," *Journal of Guidance, Control, and Dynamics*, Vol. 29, No. 6, 2006, pp. 1454–1460. doi:10.2514/1.22495

[7] Shin, J. Y., Balas, G. J., and Kaya, M. A., "Blending Methodology of Linear Parameter Varying Control Synthesis of F-16 Aircraft System," *Journal of Guidance, Control, and Dynamics*, Vol. 25, No. 6, 2002, pp. 1040–1048. doi:10.2514/2.5008

[8] Edwards, P. T., "Modern Flight Control Design, Implementation, and Flight Test," Master's Thesis, Air Force Inst. of Technology, Wright–Patterson Air Force Base, OH, 1997.

[9] Nguyen, L. T., Ogburn, M. E., Gillert, W. P., Kibler, K. S., Brown, P. W., and Deal, P. L., "Simulator Study of Stall/Post-Stall Characteristics of a Fighter Airplane with Relaxed Longitudinal Static Stability," NASA TR 1538, 1979.

[10] Garza, F. R., and Morellli, E. A., "A Collection of Nonlinear Aircraft Simulations in MATLAB," NASA TR 212145, 2003.

[11] Myers, T. T., McRuer, D. T., and Johnston, D. E., "Flying Qualities and Control System Characteristics for Superaugmented Aircraft," NASA CR-170419, 1984.

[12] McRuer, D. T., and Graham, D., "Human Pilot Dynamics in Compensatory Systems," Air Force Flight Dynamics Lab. TR-65-15, July 1965.

[13] Zhou, K., and Doyle, J. C., *Essentials of Robust Control*, Prentice–Hall, Upper Saddle River, NJ, 1998.

[14] Gahinet, P., and Apkarian, P., "A Linear Matrix Inequality Approach to H_∞ Control," *International Journal of Robust and Nonlinear Control*, Vol. 4, No. 4, 1994, pp. 421–448. doi:10.1002/rnc.4590040403

[15] Balas, G., Chiang, R., Packard, A., and Safonov, M., *Robust Control Toolbox*, Math Works, Natick, MA, 2005.

[16] Becker, G., "Additional Results on Parameter-Dependent Controllers for LPV Systems," *Proceedings of the 13th IFAC World Congress*, San Francisco, CA, 1996, pp. 351–356.

[17] Military Standard, *Flying Qualities of Piloted Aircraft*, MIL-STD-1797A, Jan. 1990.

[18] Alvarez, D. J., "Piloted Simulation Study Comparing Classical and Robust Flight Control Design Methods," Master's Thesis, California State Univ., Long Beach, CA, 2009.

[19] Klyde, D. H., "Development and Evaluation of the Smart-Cue Concept: Simulation Test Plan," Systems Technology WP-1362-3, Dec. 12, 2005.

[20] Kish, B. A., et al., "A Limited Flight Test Investigation of Pilot-Induced Oscillation due to Elevator Rate Limiting," Air Force Flight Test Center TR-97-12, June 1997.

[21] Cooper, G. E., and Harper, R. P., Jr., "The Use of Pilot Rating in the Evaluation of Aircraft Handling Qualities," AGARD Rept. 567, April 1969.

[22] Weingarten, N. C., and Chalk, C. R., "In-Flight Investigation of Large Airplane Flying Qualities for Approach and Landing," Air Force Wright Aeronautical Labs. TR-81-3118, Sept. 1981.

[23] Thompson, P. M., Klyde, D. H., Bachelder, E. N., and Rosenthal, T. J., "Development of Wavelet-Based Techniques for Detecting Loss of Control," AIAA Paper 2004-5064, Providence, RI, Aug. 2004.

[24] Klyde, D. H., Howe, J. G., and Allen, R. W., "Flight-Centered Force Cueing Metrics for the Phase 1 Real Flight Demonstration," Systems Technology WP-1386-1, 30 July 2009.

[25] Mitchell, D. G., Aponso, B. L., and Hoh, R. H., "Minimum Flying Qualities Vol. 1: Piloted Simulation of Multiple Axis Flying Qualities," Wright Research and Development Center TR-89-3125, Jan. 1990.